Application of Least Squares Stress Stabilization Method on Nodal Integration of RPIM with Tetrahedral Background Cells

***M.M. Yavuz[1] and †B. Kanber[2]**

[1] *Energy Systems Engineering Department, Osmaniye Korkut Ata University, Osmaniye, TURKEY.*

[2] *Department of Mechanical Engineering, University of Gaziantep, Gaziantep, TURKEY.*

*Presenting author: muratyavuz@osmaniye.edu.tr

†Corresponding author: kanber@gantep.edu.tr

Abstract

The authors previously show that NI-RPIM solution of 3D tetrahedral cells [Yavuz and Kanber (2015)] includes unstable stress distributions. Therefore, in this study, the fluctuations in stresses are attempted to reduce using two different algorithms; Average stress distribution (ASD) in local support domain and LSS (least square stabilization) algorithms. NI-RPIM is improved with these algorithms to solve 3D solid mechanics problems with higher order Taylor series terms in nodal integration. Integration methodology is developed based on the study of [Liu et al. (2007)]. Tetrahedral integration cells are used in the solution of 3D elasto-static problems. Order of Taylor series terms is used up to 4th order for ASD. Also effects of shape parameters (α_c and q) in RBF and support domain size (sd) are searched. The results are compared with available analytical solutions and discussed in detail.

Keywords: Nodal Integration, RPIM, Tetrahedral Background Cells, Least-Squares Stabilization

Introduction

Strain and stress formations are one of the critical design factors and always considered in machine design. Besides the working performance, strength and service life are also important in a machinery system and must be adjusted in a range of safety. A well designed mechanical system has enough strength against working loads. It been also avoided from the usage of excessive parts. For this reason, the best and optimum structural designs should be created.

It is needed to investigate the initial designs on stress analysis for optimizations. The critical locations must be determined and fixed. In general, the formation of stresses cannot be detected easily, especially for complex and non-uniform shapes. Geometry simplifications can be sometimes used with respect to analysed model. However, they include differences between analysed real model and simplified model, which causes errors. Thus, different numerical and experimental techniques have been developed for investigation with including less simplification, especially for complex shapes. Experimental techniques show responses of forces directly and reflect considerable results. However, investigation of each component or effect of parameter causes to repeat the experiment again and again.

Numerical methods can be another alternative way for investigation. On the contrary to requirements of experimental setup and apparatus in experimental investigation, numerical techniques do not need any experimental preparation, which can give fast and sensible results with respect to developed computer technology and used numerical methods. Even if it is mainly used approximate solutions, precise results can be achieved with a well-defined model. Different

numerical techniques have been developed. FDM (finite difference method), FEM (finite element method) and BEM (boundary element method) are widely used.

Unlike other methods, FEM has been very popular and used especially in the solutions of solid mechanics problems. The analysed model is divided to small elements, which are called finite elements and all solution procedure continues based on these elements. In most of the cases, formation of elements has poor shapes especially for complex geometries, which decreases accuracy of solutions. Construction of finite elements in smooth structure can consume most of analysing time. For this reason, meshfree techniques have been developed for decreasing numerical modelling time and effort. It is mainly used in early stages as SPH (smoothed particle hydrodynamics) [Gingold and Monaghan (1977); Lucy (1977)] on the solutions of astrophysical problems. DEM (diffuse element method) [Nayroles et al. (1992)] is developed at the further development stages. Mesh generation is not required, at least for interpolation. It includes MLS (moving least square) functions, which is used further development stage of EFG (element-free Galerkin) [Belytschko et al. (1994)] method. Partitions of unity [Babuska and Melenk (1996)] are developed by using MLS functions. Reproducing kernel particle method (RKPM) [Liu et al. (1996)], meshless local Petrov-Galerkin (MLPG) [Atluri and Zhu (1998)], point interpolation method (PIM) [Liu and Gu (2001)] and radial point interpolation method (RPIM) [Wang and Liu (2002a)] have been developed. Radial basis functions (RBF) are widely used in meshfree approximations, which are also used for development of BKM (boundary knot method) [Chen and Tanaka (2002)]. Also some of these methods are used in different integration methods. PIM and RPIM are further used with different methods and integration schemes; linearly conforming point interpolation method (LC-PIM) [Liu et al. (2005)], nodal integration radial point interpolation method (NI-RPIM) [Liu et al. (2007)], NS-PIM (node-based smoothed point interpolation method) [Zhang et al. (2007)], edge-based smoothed point interpolation method (ES-PIM) [Liu and Zhang (2008)] and CS-RPIM (cell-based smoothed radial point interpolation method) [Liu and Zhang (2009)] are available in literature.

Different techniques and methods can be combined for increasing the applicability of these methods. One of the integration schemes; nodal integration schemes can increase applicability and be effective for compact usage inside of RPIM, which is explained in detail in the study of Liu et al. (2007). This method uses Taylor series expansion in integration and the solution results are mainly affected with the used order of Taylor expansion. It is used for tetrahedral background cells [Yavuz and Kanber (2015)] on the solution of 3D elasto-static problems for increasing applicability. Each node in the model has its own tetrahedral integration cells. However it is observed that stress results include fluctuations and high values when compared with available analytical and FEM solutions. In literature, behaviour of nodal integration includes instabilities in some cases. Initially Biessel and Belytschko (1996) include additional a stabilization term on potential energy function of element-free Galerkin (EFG) method for nodal integration. It achieves instability problems of nodal integration in weak form formulations. Chen et al. (2001) also focus on instability of direct nodal integration and observe that integration constraints include errors in direct nodal integration and they cannot be satisfied enough in Gaussian integration at irregular discretization. They eliminate this problem with including a strain smoothing stabilization. Zhou et al. (2003) include square residual of equilibrium equation into potential energy function in stabilized nodal integration scheme. The used Voronoi diagram with supporting Delaunay triangles increases accuracy of volume assignment of nodal integration. Van et al. (2007) use conforming nodal integration into finite element formulation of laminate plates, which prevents shear locking. Han (2010) uses stabilized conforming nodal integration method on elasto-plastic analysis of metal forming process. Nodal integration with strain smoothing stabilization is used, which prevents instabilities of integration of Galerkin weak form formulations. Elmer et al. (2012) use a stable nodal integration

method on nearly incompressible solids. Xu (2014) uses stabilized nodal integration for cracking particles method (CPM), which supports stability and computational efficiency. Duan and Belytschko (2008) mention and compare 3 different stabilization techniques; which are least-square stabilization (LSS) [Biessel and Belytschko (1996); Fries and Belytschko (2007)], Taylor series expansion based stabilization (TEBS) [Liu et al. (1985); Nagashima (1999); Liu et al. (2007)] and the finite increment gradient stabilization (FIG) [Bonet and Kulasegaram (2000)], which can adjust stress instabilities.

In the previous study of Yavuz and Kanber (2015), it is observed that the nodal integration of radial point interpolation method (RPIM) based on Taylor series terms with tetrahedral background cells causes some fluctuations in stress results. Therefore, in this study, it is attempted to stabilize stresses using average stress distributions for local support domain of each node and least square stress stabilization method. RBF includes different shape parameters and their effects [Wang and Liu (2002b); Kanber et al. (2013); Bozkurt et al. (2013)] are also searched in some studies. They can affect solution results and suitable parameters must be searched before their usage. Effects of shape parameters (α_c and q) in RBF and support domain size (sd) are searched. The results are compared with available analytical solutions.

RPIM Shape Functions

Construction of shape functions forms an important section for FEM and meshfree methods. High qualified shape functions gives better results and includes less errors. The shape functions are mainly occurred with interpolations and a suitable interpolation method must be used for increasing accuracy.

Relation between nodes in meshfree methods is mainly obtained with interpolations. Various interpolation methods are available in literature. RPIM [Wang and Liu (2002a)] is one of interpolation technique and widely used. It includes PIM [Liu et al. (2001)] with radial basis functions. When shape functions have been constructed, a field function $u(x)$ is created and given as in Eq. (1), which is consist of polynomial and basis functions.

$$u(x)=\sum_{i=1}^{n} R_i(x)\times a_i + \sum_{j=1}^{m} P_j(x)\times b_j = R^T(x)\times a + P^T(x)\times b \tag{1}$$

$R_i(x)$ and $P_j(x)$ represent radial basis and polynomial basis functions, respectively. a_i and b_j are related constants, n is the number of field nodes in the local support domain and m is the number of polynomial terms. Interpolations between nodes are mainly accomplished within the local support domain for each node or point of interests.

Various RBF [Liu and Gu (2005); Liu (2009)] are available in literature, like multi-quadrics (MQ), the Gaussian (Exp), the thin plate spline (TSP) and logarithmic radial basis functions. MQ is [Liu and Gu (2005); Dinis et al. (2007)] used as radial basis function in Eq. (2).

$$R_i(x)=\left(r_i^2+(\alpha_c\times d_c)^2\right)^q \tag{2}$$

where d_c is usually set as average nodal spacing near the point of interest at x; α_c and q are shape parameters. It is [Liu and Gu (2005); Liu (2009)] recommended to use q as 1.03 and α_c as

3.00 for MQ basis function. The radial distance is given in Eq. (3) for 3D cases. Also the polynomial terms are given in Eq. (4) which are mainly derived from binomial expansion.

$$r_i(x) = \sqrt{(x - x_i)^2 + (y - y_i)^2 + (z - z_i)^2} \tag{3}$$

$$p^T(x) = \{1, x, y, z, x^2, xy, y^2, yz, z^2, zx, ...\} \tag{4}$$

Interpolation is applied in a support domain for point of interest. Different support domain geometries can be used, like circular, elliptical, triangular or rectangular. A circular local support domain is used and its covered area is given by radius of circle (d_s), which is given in Eq. (5).

$$d_s = \alpha_s \times d_c \tag{5}$$

where d_c is average nodal spacing and α_s is a positive real number of dimensionless size of the local support domain. Its value [Liu and Gu (2005); Dinis et al. (2007)] is commonly used between 2.00 and 3.00. The unknown constants of field function of a_i and b_j in Eq. (1) can be determined by enforcing the field function to pass through all n field nodes in the local support domain. At the k^{th} point or last point in a local support domain, field function can be written as:

$$u(x_k, y_k, z_k) = \sum_{i=1}^{n} R_i(x_k, y_k, z_k) \times a_i + \sum_{j=1}^{m} P_j(x_k, y_k, z_k) \times b_j \qquad k=1,2,..n \tag{6}$$

The matrix form of Eq. (6) can be expressed as

$$U_e = R_q \times a + P_m \times b = \{u_1\ u_2\ ...u_n\}^T \tag{7}$$

where U_e is the vector of function values at the nodes in the local support domain. R_q is the moment matrix of RBF and P_m is the polynomial moment matrix [Liu and Gu (2005)], which are given in Eq. (8) and (9), respectively.

$$R_q = \begin{bmatrix} R_1(r_1) & R_2(r_1) & ... & R_n(r_1) \\ R_1(r_2) & R_2(r_2) & ... & R_n(r_2) \\ ... & ... & ... & ... \\ R_1(r_n) & R_2(r_n) & ... & R_n(r_n) \end{bmatrix}_{(n \times n)} \tag{8}$$

$$P_m = \begin{bmatrix} 1 & x_1 & y_1 & z_1 & ... & P_m(r_1) \\ 1 & x_2 & y_2 & z_2 & ... & P_m(r_2) \\ ... & ... & ... & ... & ... & ... \\ 1 & x_n & y_n & z_n & ... & P_m(r_n) \end{bmatrix}_{(n \times m)} \tag{9}$$

a and b are vectors of unknown coefficients for radial and polynomial basis functions respectively. They are given in Eq. (10) and (11).

$$a^T = \{a_1\ a_2\ ...a_n\} \tag{10}$$

$$b^T = \{b_1\ b_2\ ...b_n\} \tag{11}$$

For solution of field function, unknown parameter a in Eq. (7) must satisfy in polynomial function,

$$\sum_{j=1}^{n} p_j(x_i) \times a_i = P_m^T \times a = 0 \quad \text{j=1,2,..,m} \tag{12}$$

Combination of Eq. (7) and Eq. (1) yields the following equations in the matrix form:

$$\tilde{U}_e = \begin{bmatrix} U_e \\ 0 \end{bmatrix} = \begin{bmatrix} R_q & P_m \\ P_m^T & 0 \end{bmatrix} \begin{Bmatrix} a \\ b \end{Bmatrix} = G \times\ a_0 \quad \text{j=1,2,..,m} \tag{13}$$

where

$$\tilde{U}_e = \begin{bmatrix} U_e \\ 0 \end{bmatrix} = \{a_1\ a_2\ ...a_n\ 0\,0\,...0\}^T \tag{14}$$

Unique solution is obtained if inverse of matrix G exists:

$$a_0 = \begin{Bmatrix} a \\ b \end{Bmatrix} = G^{-1} \times \tilde{U}_e \tag{15}$$

Substituting Eq. (15) into Eq. (1), interpolation with respect to field function can be expressed as,

$$u(x) = \left\{R^T(x) \times P^T(x)\right\} \times G^{-1} \times \tilde{U}_e = \tilde{\varphi}(x) \times \tilde{U}_e \tag{16}$$

Finally [Liu and Gu (2005); Dinis et al. (2007)], RPIM shape functions for the corresponding n field nodes can be obtained as

$$\varphi^T(x) = \{\varphi_1(x)\,\varphi_2(x)...\varphi_n(x)\} \tag{17}$$

The approximation function can be written as

$$u(x) = \varphi^T(x) \times U_e = \sum_{i=1}^{n} \varphi_i \times u_i \tag{18}$$

The derivatives of $u(x)$ can be easily obtained as

$$u_{i,k}(x) = \varphi_{,k}^T(x) \times U_e \tag{19}$$

where k denotes the coordinates x, y or z. Partial differentiation is taken with respect to that defined coordinated by k.

3D Nodal Integration with Taylor Series Expansion

The approximated solution must be adapted to equilibrium equation with respect to applied boundary conditions. General form of equilibrium equation [Liu and Gu (2005); Liu et al. (2007)] and natural and essential boundary conditions are given in Eq. (21), (22) and (23), respectively.

$$L^T \times \sigma + b = 0 \tag{20}$$

$$\sigma \cdot n = \bar{t} \ \ on \ \ \tau_i \tag{21}$$

$$u = \bar{u} \ \ on \ \ \tau_u \tag{22}$$

L^T is [Liu and Gu (2005)] differential operator, σ is the stress vector, u is the displacement vector, b is the body force vector, $\bar{t}$ is prescribed traction on the natural boundaries, $\bar{u}$ is prescribed displacement on the essential boundaries and n is the vector of unit outward normal on the natural boundary. L^T, σ, u and b are given in Eq. (23), (24), (25) and (26) respectively.

$$L^T = \begin{bmatrix} \partial/\partial x & 0 & 0 & 0 & \partial/\partial z & \partial/\partial y \\ 0 & \partial/\partial y & 0 & \partial/\partial z & 0 & \partial/\partial x \\ 0 & 0 & \partial/\partial z & \partial/\partial y & \partial/\partial x & 0 \end{bmatrix} \tag{23}$$

$$\sigma^T = \begin{bmatrix} \sigma_{xx} & \sigma_{yy} & \sigma_{zz} & \tau_{yz} & \tau_{xz} & \tau_{xy} \end{bmatrix} \tag{24}$$

$$u = \begin{bmatrix} u \\ v \\ w \end{bmatrix} \tag{25}$$

$$b = \begin{bmatrix} b_x \\ b_y \\ b_z \end{bmatrix} \tag{26}$$

Equilibrium equation and natural and essential boundary conditions are represented with respect to weak form formulation in RPIM. Hence, the equilibrium equation, Eq. (20) can be defined as in Galerkin weak formulation in Eq. (27),

$$\int (L \times \delta u)^T \times (D \times L \times u) d\Omega - \int (\delta u^T \times b) d\Omega - \int (\delta u^T \times t) d\Gamma = 0 \tag{27}$$

D matrix is material coefficient matrix and it is given for isotropic solids as;

$$D=\frac{E\times(1-\nu)}{(1+\nu)\times(1-2\nu)}\times\begin{bmatrix} 1 & \frac{\nu}{1-\nu} & \frac{\nu}{1-\nu} & 0 & 0 & 0 \\ \frac{\nu}{1-\nu} & 1 & \frac{\nu}{1-\nu} & 0 & 0 & 0 \\ \frac{\nu}{1-\nu} & \frac{\nu}{1-\nu} & 1 & 0 & 0 & 0 \\ 0 & 0 & 0 & \frac{1-2\nu}{2\times(1-\nu)} & 0 & 0 \\ 0 & 0 & 0 & 0 & \frac{1-2\nu}{2\times(1-\nu)} & 0 \\ 0 & 0 & 0 & 0 & 0 & \frac{1-2\nu}{2\times(1-\nu)} \end{bmatrix} \tag{28}$$

where E is Young's modulus and ν is Poisson's ratio [Liu and Gu (2005)]. When substituting the approximated function in Eq. (18), into Eq. (27), general form of stiffness and force matrices are obtained.

$$K\times u=f \tag{29}$$

In Eq. (30), stiffness matrix formulation is represented. Force matrix formulation is given in Eq. (31). In addition, strain matrix, which includes derivatives of shape functions, is given in Eq. (32).

$$K_{ij}=\int B_i^T\times D\times B_j d\Omega \tag{30}$$

$$f_i=\int \varphi_i\times t d\Gamma+\int \varphi_i\times b d\Omega \tag{31}$$

$$B_i=\begin{bmatrix} \varphi_{i,x} & 0 & 0 \\ 0 & \varphi_{i,y} & 0 \\ 0 & 0 & \varphi_{i,z} \\ 0 & \varphi_{i,z} & \varphi_{i,y} \\ \varphi_{i,z} & 0 & \varphi_{i,x} \\ \varphi_{i,y} & \varphi_{i,x} & 0 \end{bmatrix} \tag{32}$$

A suitable integration method is needed to solve these equations. Various integration techniques are available. In NI-RPIM [Liu et al. (2007)], a series integration scheme is used with Taylor series. Series are widely used in mathematical operations, especially in numerical studies. An unknown value of a valid function can be estimated with a known value with series operations. One of the series is Taylor series and it is widely used in computational fluid dynamics with respect to finite difference method (FDM). An example of value estimation from x_0 to x_0+h can be defined serial expansion of functions and it is given in Eq. (33). R_n is the total error between value of $f(x_0+h)$ and its Taylor expansion results. In general, the degree of used terms in FDM increases the accuracy. In Eq. (33), Taylor series are expanded and derived to n^{th} order.

$$f(x_0+h)=f(x_0)+\frac{f'(x_0)}{1!}\times h+\frac{f''(x_0)}{2!}\times h^2+\frac{f'''(x_0)}{3!}\times h^3+...+\frac{f^n(x_0)}{n!}\times h^n+R_n \tag{33}$$

Equations of integrations are expanded with respect to Taylor series expansion as Eq. (33). Stiffness matrix is set as approximate function as $f(x,y,z)$, which is given in Eq. (34),

$$\begin{aligned}f(x,y,z)=& f(x_0,y_0,z_0)+(x-x_0)\times\frac{\partial f(x_0,y_0,z_0)}{\partial x}+(y-y_0)\times\\ &\frac{\partial f(x_0,y_0,z_0)}{\partial y}+(z-z_0)\times\frac{\partial f(x_0,y_0,z_0)}{\partial z}+\frac{1}{2!}\times(x-x_0)^2\times\\ &\frac{\partial f^2(x_0,y_0,z_0)}{\partial x^2}+\frac{1}{2!}\times 2\times(x-x_0)\times(y-y_0)\times\frac{\partial f^2(x_0,y_0,z_0)}{\partial x\partial y}+\\ &\frac{1}{2!}\times(y-y_0)^2\times\frac{\partial f^2(x_0,y_0,z_0)}{\partial y^2}+\frac{1}{2!}\times 2\times(y-y_0)\times(z-z_0)\times\\ &\frac{\partial f^2(x_0,y_0,z_0)}{\partial y\partial z}+\frac{1}{2!}\times(z-z_0)^2\times\frac{\partial f^2(x_0,y_0,z_0)}{\partial z^2}+\frac{1}{2!}\times 2\times\\ &(z-z_0)\times(x-x_0)\times\frac{\partial f^2(x_0,y_0,z_0)}{\partial z\partial x}+\frac{1}{3!}\times(x-x_0)^3\times\\ &\frac{\partial f^3(x_0,y_0,z_0)}{\partial x^3}+\frac{1}{3!}\times(y-y_0)^3\times\frac{\partial f^3(x_0,y_0,z_0)}{\partial y^3}+\frac{1}{3!}\times(z-z_0)^3\times\\ &\frac{\partial f^3(x_0,y_0,z_0)}{\partial z^3}+\frac{1}{3!}\times 3\times(x-x_0)^2\times(y-y_0)\times\frac{\partial f^3(x_0,y_0,z_0)}{\partial x^2\partial y}+...\end{aligned} \tag{34}$$

The nodal integration of Eq. (34) can be written as Eq. (35),

$$\begin{aligned}\int f(x,y,z)d\Omega=\int(& f(x_0,y_0,z_0)+(x-x_0)\times\frac{\partial f(x_0,y_0,z_0)}{\partial x}+(y-y_0)\times\\ &\frac{\partial f(x_0,y_0,z_0)}{\partial y}+(z-z_0)\times\frac{\partial f(x_0,y_0,z_0)}{\partial z}+\frac{1}{2!}\times(x-x_0)^2\times\frac{\partial f^2(x_0,y_0,z_0)}{\partial x^2}+\\ &\frac{1}{2!}\times 2\times(x-x_0)\times(y-y_0)\times\frac{\partial f^2(x_0,y_0,z_0)}{\partial x\partial y}+\frac{1}{2!}\times(y-y_0)^2\times\frac{\partial f^2(x_0,y_0,z_0)}{\partial y^2}+\\ &\frac{1}{2!}\times 2\times(y-y_0)\times(z-z_0)\times\frac{\partial f^2(x_0,y_0,z_0)}{\partial y\partial z}+\frac{1}{2!}\times(z-z_0)^2\times\frac{\partial f^2(x_0,y_0,z_0)}{\partial z^2}+\\ &\frac{1}{2!}\times 2\times(z-z_0)\times(x-x_0)\times\frac{\partial f^2(x_0,y_0,z_0)}{\partial z\partial x}+\frac{1}{3!}\times(x-x_0)^3\times\frac{\partial f^3(x_0,y_0,z_0)}{\partial x^3}+\\ &\frac{1}{3!}\times(y-y_0)^3\times\frac{\partial f^3(x_0,y_0,z_0)}{\partial y^3}+\frac{1}{3!}\times(z-z_0)^3\times\frac{\partial f^3(x_0,y_0,z_0)}{\partial z^3}+\frac{1}{3!}\times 3\times\\ &(x-x_0)^2\times(y-y_0)\times\frac{\partial f^3(x_0,y_0,z_0)}{\partial x^2\partial y}+...)d\Omega\end{aligned} \tag{35}$$

If Eq. (35) is separated and arranged, the following form can be obtained,

$$\begin{aligned}\int f(x,y,z)d\Omega = \int f(x_0,y_0,z_0)d\Omega + \int (x-x_0)\times\frac{\partial f(x_0,y_0,z_0)}{\partial x}d\Omega + \int (y-y_0)\times \\ \frac{\partial f(x_0,y_0,z_0)}{\partial y}d\Omega + \int (z-z_0)\times\frac{\partial f(x_0,y_0,z_0)}{\partial z}d\Omega + \int \frac{1}{2!}\times(x-x_0)^2 \times \\ \frac{\partial f^2(x_0,y_0,z_0)}{\partial x^2}d\Omega + \int \frac{1}{2!}\times 2\times(x-x_0)\times(y-y_0)\times\frac{\partial f^2(x_0,y_0,z_0)}{\partial x\partial y}d\Omega + \\ \int \frac{1}{2!}\times(y-y_0)^2\times\frac{\partial f^2(x_0,y_0,z_0)}{\partial y^2}d\Omega + \int \frac{1}{2!}\times 2\times(y-y_0)\times(z-z_0)\times \\ \frac{\partial f^2(x_0,y_0,z_0)}{\partial y\partial z}\mathrm{d}\Omega + \int \frac{1}{2!}\times(z-z_0)^2\times\frac{\partial f^2(x_0,y_0,z_0)}{\partial z^2}d\Omega + \int \frac{1}{2!}\times 2\times \\ (z-z_0)\times(x-x_0)\times\frac{\partial f^2(x_0,y_0,z_0)}{\partial z\partial x}d\Omega + \int \frac{1}{3!}\times(x-x_0)^3\times\frac{\partial f^3(x_0,y_0,z_0)}{\partial x^3} \\ d\Omega + ...\end{aligned} \tag{36}$$

$$\begin{aligned}\int f(x,y,z)d\Omega = f(x_0,y_0,z_0)\times\int 1d\Omega + f_x(x_0,y_0,z_0)\times\int (x-x_0)d\Omega + \\ f_y(x_0,y_0,z_0)\times\int (y-y_0)d\Omega + f_z(x_0,y_0,z_0)\times\int (z-z_0)d\Omega + \\ f_{xx}(x_0,y_0,z_0)\times\frac{1}{2!}\times\int (x-x_0)^2 d\Omega + f_{xy}(x_0,y_0,z_0)\times \\ \int (x-x_0)\times(y-y_0)d\Omega + ...\end{aligned} \tag{37}$$

In Eq. (37), $x-x_0$ represents Δx, $y-y_0$ represents Δy and $z-z_0$ represents Δz. The distance is calculated from midpoint of related field node and integration cell, which is called Taylor integration cells. $d\Omega$ is equal to volume of Taylor integration cell. Each Taylor integration cell for each field node includes a volume that does not interact with other field nodes of Taylor integration cells.

Integration with Tetrahedral Shaped Taylor Integration Cells

It is required in NI-RPIM [Liu et al. (2007)] to construction of integration domains for each node in the analysed model. These domains should not coincide with each other and must be fully integrated. Taylor integration domains are constructed with irregular tetrahedral geometries for irregular distributed nodes. These irregular domain construction supports to more flexible domains, rather than hexahedral cells. Delaunay triangulation method is used for creating tetrahedral cells between nodes by using MATLAB.

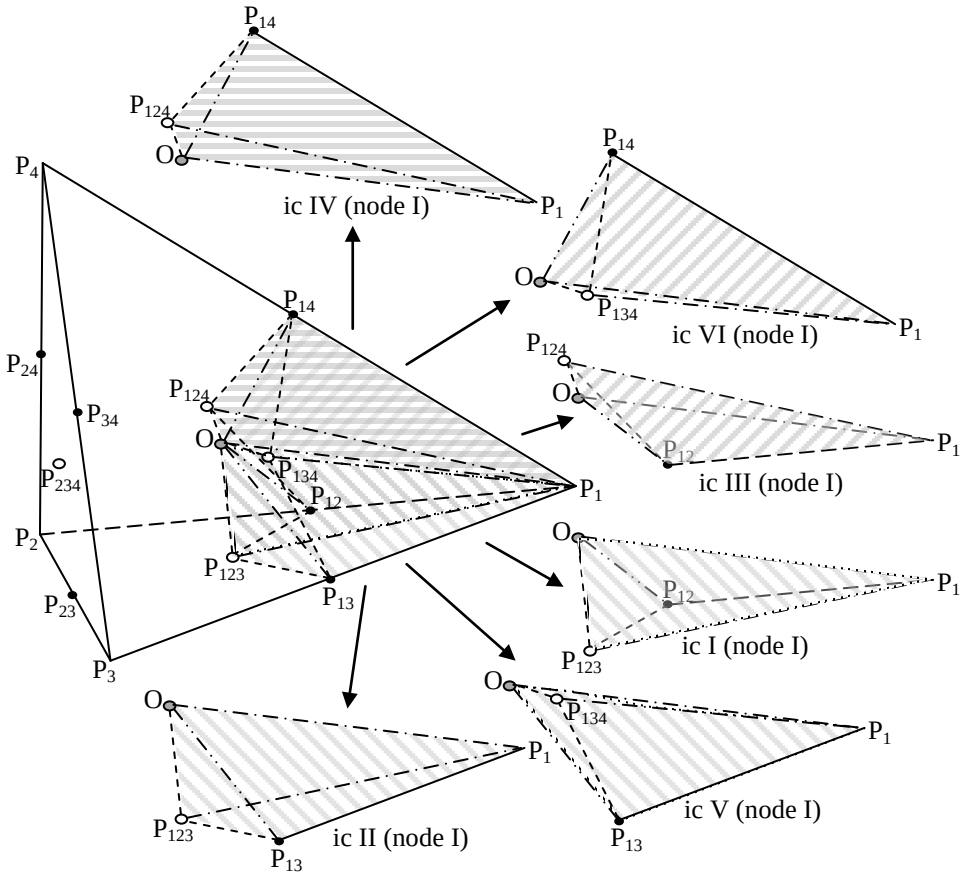

Figure 1. Sub-division of tetrahedral background cell for each node.

In Fig. 1, a tetrahedral background cell is given. The cell which is formed by field nodes of P_1 (x_1,y_1,z_1), P_2 (x_2,y_2,z_2), P_3 (x_3,y_3,z_3) and P_4 (x_4,y_4,z_4) is further divided into 6 different integration cells (ic I, II...). So, the total number of integration cells for a field node can be calculated by multiplying 6 by the number of tetrahedral cells that are connected to the field node. P_{12}, P_{13}, P_{14}, P_{23}, P_{24} and P_{34} are centre point of each side line of tetrahedral cell. P_{123}, P_{124}, P_{134} and P_{234} are centre points of surface areas. O is the centre point.

Table 1. Components of edges for subdivided Taylor Integration cells for each node.

	integration cell (ic)	components of edges					integration cell (ic)	components of edges			
Node I (P1)	I	P_1	P_{12}	P_{123}	O	Node III (P3)	I	P_3	P_{13}	P_{123}	O
	II	P_1	P_{123}	P_{13}	O		II	P_3	P_{123}	P_{23}	O
	III	P_1	P_{124}	P_{12}	O		III	P_3	P_{134}	P_{13}	O
	IV	P_1	P_{14}	P_{124}	O		IV	P_3	P_{34}	P_{134}	O
	V	P_1	P_{13}	P_{134}	O		V	P_3	P_{23}	P_{234}	O
	VI	P_1	P_{134}	P_{14}	O		VI	P_3	P_{234}	P_{34}	O
Node II (P2)	I	P_2	P_{123}	P_{12}	O	Node IV (P4)	I	P_4	P_{124}	P_{14}	O
	II	P_2	P_{23}	P_{123}	O		II	P_4	P_{24}	P_{124}	O
	III	P_2	P_{12}	P_{124}	O		III	P_4	P_{14}	P_{134}	O
	IV	P_2	P_{124}	P_{24}	O		IV	P_4	P_{134}	P_{34}	O
	V	P_2	P_{234}	P_{23}	O		V	P_4	P_{234}	P_{24}	O
	VI	P_2	P_{24}	P_{234}	O		VI	P_4	P_{34}	P_{234}	O

Subdivision of tetrahedral integration cell components for each node is tabulated in Table 1. Subdivision of tetrahedral cell can cause negative volumes [Toron (2004); Kovalev (2005)]. Therefore, the orientation of subdivided cell nodes is placed with an order of preventing negative volume results.

In Eq. (37), the integrations $\int 1 d\Omega$, $\int (\Delta x) d\Omega$, $\int (\Delta y) d\Omega$, $\int (\Delta z) d\Omega$, $\int (\Delta x^2) d\Omega$ … must be calculated for tetrahedral background cells. The first integration represents the volume of tetrahedron and can also be calculated as determinant of edge distances [Bhowmick and Shontz (2012)] in Eq. (38).

$$Volume = \frac{1}{6} \cdot \begin{vmatrix} x_2 - x_1 & x_3 - x_1 & x_4 - x_1 \\ y_2 - y_1 & y_3 - y_1 & y_4 - y_1 \\ z_2 - z_1 & z_3 - z_1 & z_4 - z_1 \end{vmatrix} \tag{38}$$

However, integration of volume in terms of $x, y, z, x^2, ...$ includes complex operations for irregular tetrahedral shapes. Hence, geometry can be transformed into natural coordinates by using Jacobian transformation. In Fig. 2, the transformation of tetrahedron geometry from global to natural coordinates is shown for ic II of field node I. P_1', P_{123}', P_{13}' and O' represent the transformed natural coordinates from global coordinates of P_1, P_{123}, P_{13} and O points, respectively. Also for other integration cells, P_1', P_{123}', P_{13}' and O' in Fig. 2 correspond to second, third, fourth and fifth columns in Table 1 respectively.

The bounds of integral starts from zero to upper natural coordinate. Hence P_1, P_2, P_3 and P_4 are placed at P_1' in integral calculations. This condition can provide to no usage of parallel axis theorem to carry integration results to related edge node. Hence, x_1, y_1 and z_1 in Eq. (39), (40) and (41) are assigned x, y and z coordinates of P_1, P_2, P_3 and P_4 in related integral node calculation.

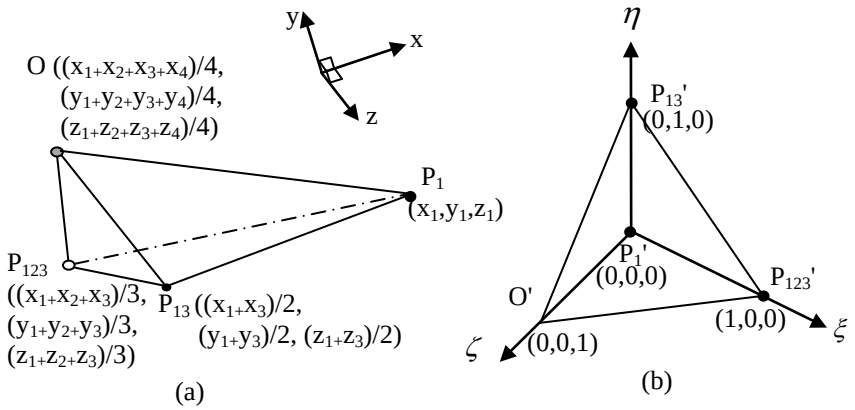

Figure 2. Transformation of an integration cell (ic II in Fig.1) from global (a) to natural (b) coordinates.

The transformation of coordinates is given in Eq. (39), (40) and (41) [Bhowmick and Shontz (2012)]. η, ξ and ζ are natural coordinates.

$$x = x_1 + (x_2 - x_1) \cdot \xi + (x_3 - x_1) \cdot \eta + (x_4 - x_1) \cdot \zeta \tag{39}$$

$$y = y_1 + (y_2 - y_1) \cdot \xi + (y_3 - y_1) \cdot \eta + (y_4 - y_1) \cdot \zeta \tag{40}$$

$$z = z_1 + (z_2 - z_1)\cdot\xi + (z_3 - z_1)\cdot\eta + (z_4 - z_1)\cdot\zeta \tag{41}$$

Determinant of Jacobian (J) transformation matrix are given in Eq. (42).

$$DET(J) = \begin{vmatrix} \frac{\partial x}{\partial \xi} & \frac{\partial x}{\partial \eta} & \frac{\partial x}{\partial \zeta} \\ \frac{\partial y}{\partial \xi} & \frac{\partial y}{\partial \eta} & \frac{\partial y}{\partial \zeta} \\ \frac{\partial z}{\partial \xi} & \frac{\partial z}{\partial \eta} & \frac{\partial z}{\partial \zeta} \end{vmatrix} = 6\cdot Volume \tag{42}$$

The transformation of integration of uniform geometry in natural coordinates is given in Eq. (43). Its application to tetrahedron geometry is given in Eq. (44). Hence integration in terms of $x, y, z, x^2, \cdots$ can be easily calculated as follows:

$$\int f(x,y,z)d\Omega = \int f\left[x(\xi,\eta,\zeta), y(\xi,\eta,\zeta), z(\xi,\eta,\zeta)\right] * \left|DET(J)\right| d\Omega' \tag{43}$$

$$\int_D f(x,y,z)dD = \left|DET(J)\right| * \int_0^1 d\xi \int_0^{1-\xi} d\eta \int_0^{1-\xi-\eta} f\left[x(\xi,\eta,\zeta), y(\xi,\eta,\zeta), z(\xi,\eta,\zeta)\right] d\zeta \tag{44}$$

Even if suitable orientation is used in Table 1, in some cases node coordinate orientations can be changed with respect to construction of tetrahedral cells in Delaunay triangulation technique. Its symptoms can be determined with negative value of determinant of Jacobian matrix. For this reason, upper integration bounds in Eq. (44) are updated with respect to where the subdivided tetrahedral cell exists, which are given in Table 2.

Table 2. Direction of tetrahedral cell and used bounds of integral in natural coordinates.

	Δx_{12}	Δy_{13}	Δz_{14}	$\int_0^{[]} f[x,y,z]d\zeta$	$\int_0^{[]} f[x,y,z]d\eta$	$\int_0^{[]} f[x,y,z]d\xi$
I	+	+	+	$1-\xi-\eta$	$1-\xi$	+1
II	+	+	-	$-(1-\xi-\eta)$	$1-\xi$	+1
III	+	-	+	$1-\xi+\eta$	$-(1-\xi)$	+1
IV	+	-	-	$-(1-\xi+\eta)$	$-(1-\xi)$	+1
V	-	+	+	$1+\xi-\eta$	$1+\xi$	–1
VI	-	+	-	$-(1+\xi-\eta)$	$1+\xi$	–1
VII	-	-	+	$1+\xi+\eta$	$-(1+\xi)$	–1
VIII	-	-	-	$-(1+\xi+\eta)$	$-(1+\xi)$	–1

Where Δx_{12} is the sign of difference between $x_2 - x_1$, Δy_{13} is the sign of difference between $y_3 - y_1$ and Δz_{14} is the sign of difference between $z_4 - z_1$ for each sub-divided integration cell. The signs of η, ξ and ζ in Eq. (39), (40) and (41) is also regulated with respect to signs of Δx_{12}, Δy_{13} and Δz_{14}.

These calculations are applied for each tetrahedral cell and the results are summed for the corresponding field node. Hence, a node includes more than one tetrahedral integration cells, which looks like a polyhedron geometry. However, all main structure of integrations is carried on each subdivided tetrahedral cells for related nodes.

Application of Stress Stabilizations

The application of nodal integration is fast and suitable for complex geometries. However, in the previous study of Yavuz and Kanber (2015), the stress results of pure/unstabilized nodal integration include high fluctuations. Even if two close nodes are selected, their stress results can be highly different. Hence application of different methods is investigated for trying to decrease the stress fluctuations.

Average Stress Distribution for Each Local Support Domain

In the previous study [Yavuz and Kanber (2015)], it is observed in nodal integration that high stress fluctuations occur at far away from application locations of force and boundary conditions. It is not expected that formation of these high fluctuations occur at that conditions with respect to Saint Vernant's principle.

For decreasing the fluctuations, average stress distributions are taken for each local support domain. The stresses of nodes in a local support domain of a related node is summed and averaged for number of nodes in that support domain.

Stiffness Effect on Boundary Locations

In the previous study [Yavuz and Kanber (2015)], some stress peak points are observed, especially on the application location of boundary conditions. Hence local stiffness matrix of nodes on boundary condition locations are changed for decreasing stress peak points. Its effects are investigated.

Least Square Stabilization

In order to decrease fluctuations, least square stabilization method (LSS) [Biessel and Belytschko (1996), Fries and Belytschko (2007), Duan and Belytschko (2008)] is used in nodal integration scheme. This method adds two equations (K^{γ} and f^{γ}) in Galerkin weak form of governing equation for providing stress stabilization. The main governing equation is previously given in Eq. 20. Addition of stress stabilization equations and detail transformation operations about governing equations can be reached from the study of Duan and Belytschko (2008). The simplified equation is given in Eq. 45. K^{γ} and f^{γ} equations are given in Eq. 46 and 47.

$$\left(K + K^{\gamma} + \beta K^{P}\right)d = \left(f + f^{\gamma} + \beta f^{P}\right) \tag{45}$$

$$K^{\gamma} = \int_{\Omega} \gamma\left(L^{T} DLN\right)^{T}\left(L^{T} DLN\right)D\Omega \tag{46}$$

$$f^{\gamma} = -\int_{\Omega} \gamma\left(L^{T} DLN\right)^{T} bD\Omega \tag{47}$$

γ is the stabilization parameter and it is given in Eq. 48.

$$\gamma = \frac{2\alpha_s l_c^2}{E} \tag{48}$$

α_s is the dimensionless stabilization parameter and used as 0.3 in this study. l_c is used as nodal spacing, which is nearly equal to 0.04*L/100.

Solution and Discussion

A cantilever beam problem is examined for investigation of stress stabilization methods. The nodal integration of RPIM is mainly prepared with respect to the study of Liu. et al. (2007). The solutions of formulations, creation of tetrahedral integration cells and subdivision calculations are accomplished with MATLAB.

The geometry and meshfree model is given in Fig. 3. The used beam has a length of 1.0 m with square section of 0.1m × 0.1m. The used meshfree model has 878 irregularly distributed nodes.

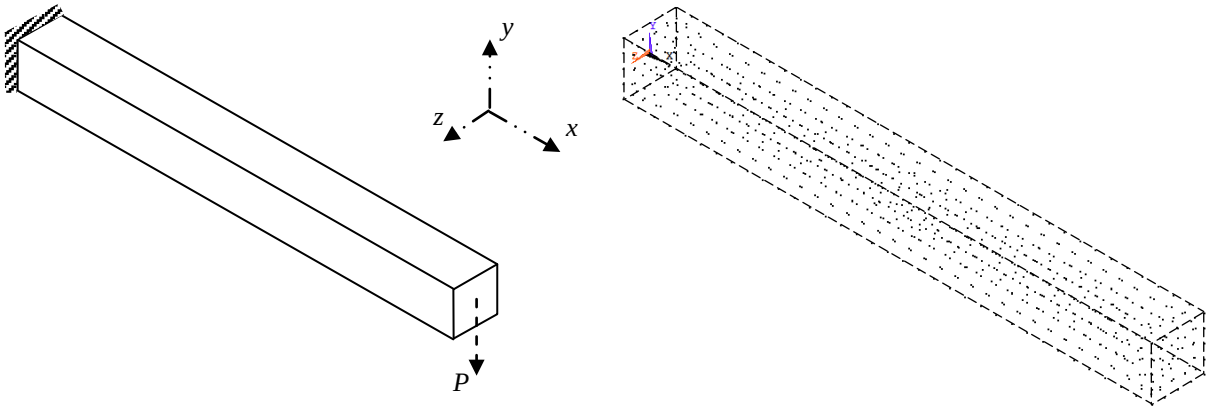

Figure 3. The used cantilever beam model geometry and meshfree model

The used material properties have linear elastic behaviour with a Young's Modulus of 200 GPa and Poisson's ratio of 0.0. The selection of Poisson's ratio as 0.0 is aimed for providing similar conditions as analytical solutions. Applied force (P) is used as 29000 N and other side of force application location is determined as application of boundary condition location. This location is fixed.

Vertical deflection equation [Beer et al. (2009)] of cantilever beam is given in Eq. 49. Where P is applied force, x is distance from fixed support location, E is Young's Modulus and I represents inertia of beam.

$$y = \frac{P \times x^2}{6 \times E \times I}(3 \times L - x) \tag{49}$$

The bending stress at upper and lower surfaces of beam is given as;

$$\sigma = \frac{M \times c}{I} \tag{50}$$

c is the distance between upper/lower surface and natural axis of the beam. In meshfree solutions, α_c is used as 3.00, dimensionless support domain size (α_s) parameter is used as 1.30 and q is used as 1.03 as default parameters.

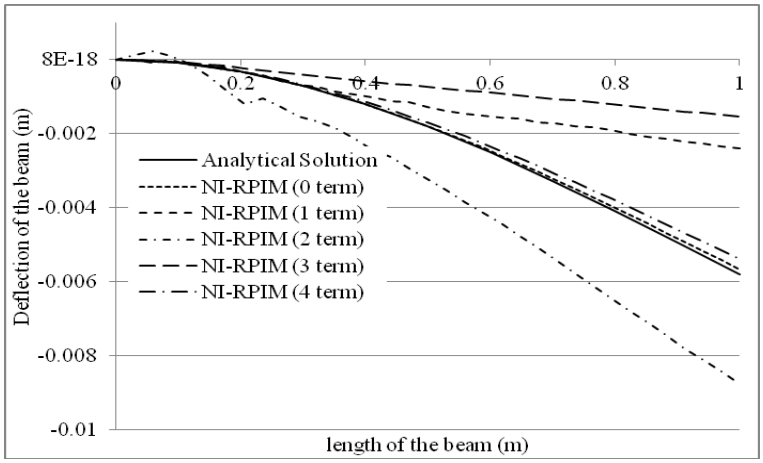

Figure 4. Comparison of deflection results of cantilever beam for analytical and pure nodal int. technique.

Deflection results of cantilever beam is shown in Fig. 4 for NI-RPIM with 0^{th}, 1^{st}, 2^{rd}, 3^{rd} and 4^{th} order Taylor terms. It is observed that 0^{th} and 4^{th} order terms give the best results when they are compared with analytical solution. There is no fluctuation occurs on deflection results of these order terms. However the used other terms includes less accuracy and small distortions at the results.

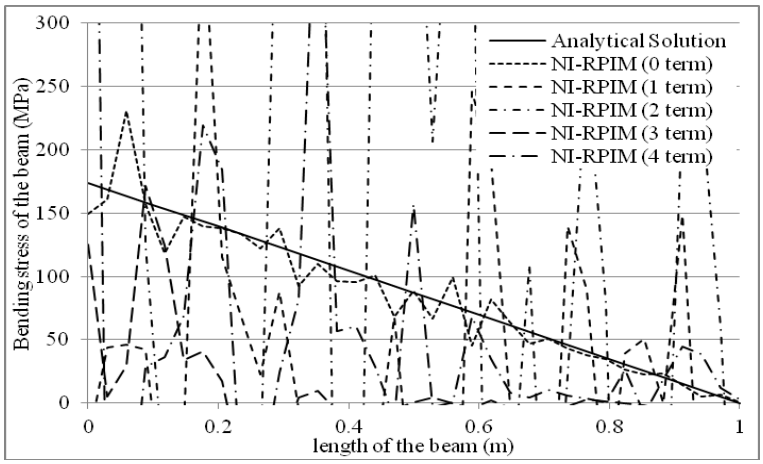

Figure 5. Comparison of bending stress results of cantilever beam for analytical and pure/unstabilized nodal int. technique.

The bending stress results are given in Fig. 5 for pure/unstabilized nodal integration, which include highly fluctuation results. The best results achieved with 0^{th} order terms, when results of all terms

are compared with each other. The stress results of 1st and 4th order terms include high stress values at the application locations of boundary conditions.

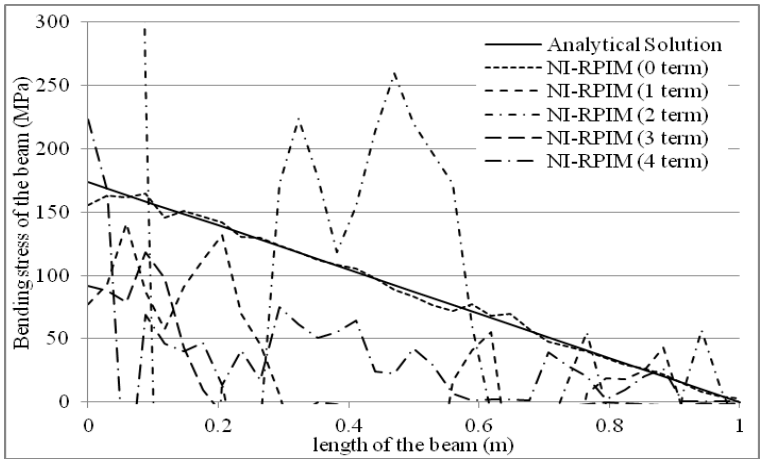

Figure 6. Comparison of bending stress results of cantilever beam for analytical and nodal int. technique with ASD.

The formation of stress results are given in Fig. 6, when averaged stress distribution (ASD) of local support domain method is applied for each node. It is observed that fluctuations of stress results are decreased. The best accuracy is achieved with the usage of 0th order term. However, results of higher terms without 0th order term have poor accuracy and include fluctuations.

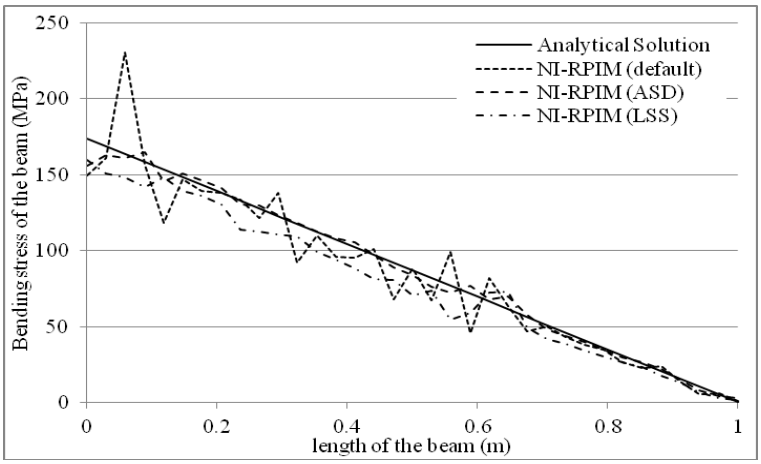

Figure 7. Comparison of bending stress results of cantilever beam for analytical and nodal int. technique of 0th order term with ASD and LSS.

In Fig.7, only the usage of 0th order term results of NI-RPIM are compared with unstabilized, ASD and LSS methods. It is observed that the usage of both stress stabilization methods decreases fluctuations in the results.

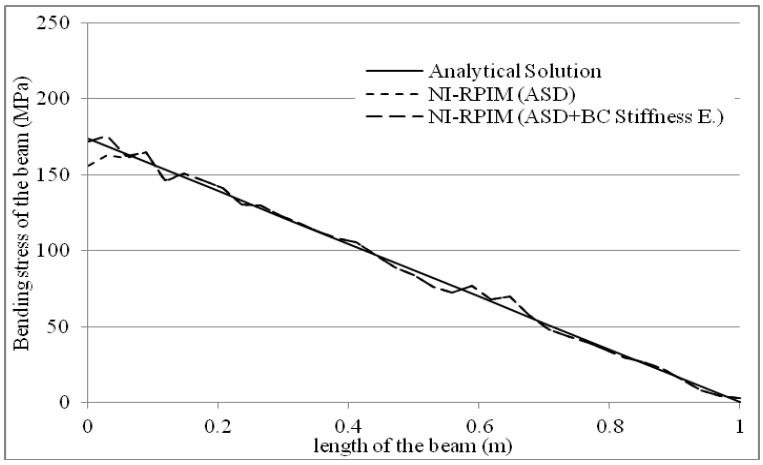

Figure 8. Comparison of bending stress results of cantilever beam for analytical and nodal int. technique of 0^{th} order term with ASD/ASD+BC Stiffness E.

NI-RPIM results of 0^{th} order term have a difference from analytical solution at the application location of boundary conditions (BC). NI-RPIM results have less stress values than analytical solution at BC. Hence, the stiffness values are decreased about %30 at this location for achieving same results at BC.

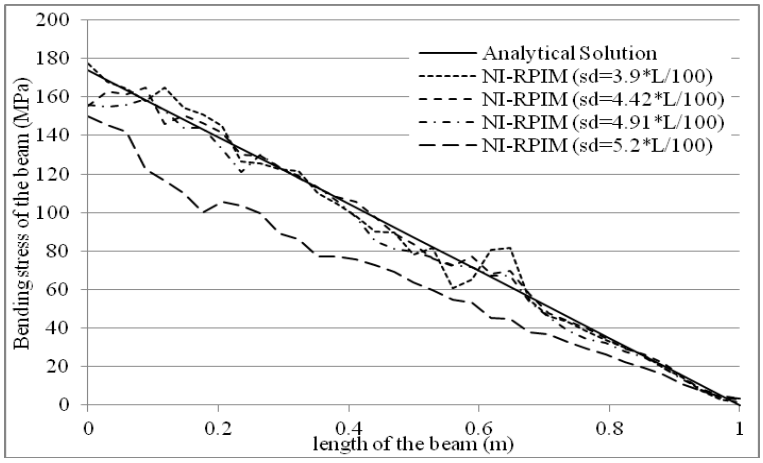

Figure 9. Comparison of effect of sd on bending stress results of cantilever beam for nodal int. with ASD (0^{th} order term).

Effect of support domain (sd) size is shown for 0^{th} order term results of NI-RPIM with ASD. When sd value of 3.9*L/100 is used, there is high fluctuation occurs about at a beam length of 0.6 m. sd size of 4.42*L/100 gives better stress results, which is used default in other solutions in this study. The average number of nodes in the local support domains is approximately equal to 44. When sd is increased, the accuracy begins decreasing.

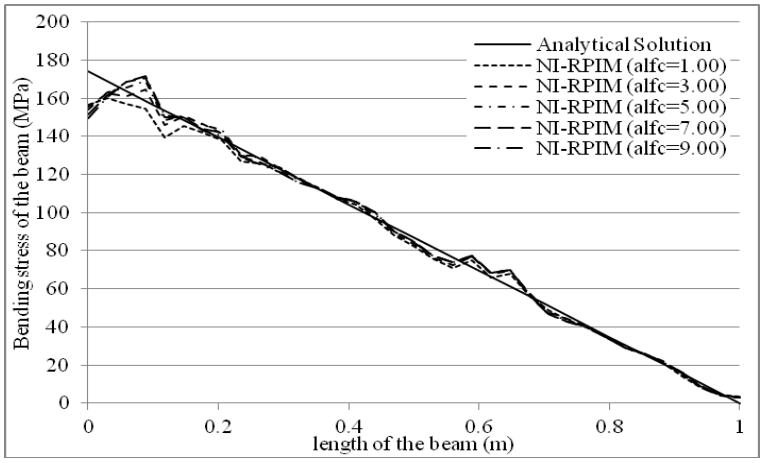

Figure 10. Comparison of effect of alfc (α_c) on bending stress results of cantilever beam for nodal int. with ASD (0^{th} order term).

Effect of alfc (α_c) results are given in Fig. 10. The only dominant effect is shown at BC and its near locations. Different alfc (α_c) results have similar characteristics.

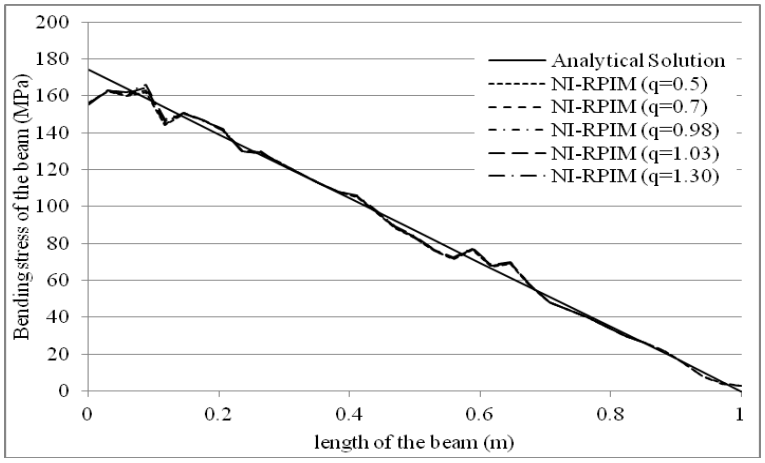

Figure 11. Comparison of effect of q on bending stress results of cantilever beam for nodal int. with ASD (0^{th} order term).

Effect of q results is given in Fig. 11. Nearly all the results of different q values have same values.

Conclusions

Tetrahedral background cells are used for the nodal integration of RPIM. The fluctuation problem in stress results of nodal integration is investigated with application of different methods. Averaged stress distribution (ASD) on local support domain and least square stabilization (LSS) methods are used. Effect of orders of Taylor terms, support domain size and RBF terms are investigated at NI-RPIM with ASD.

Results can be summarized as follows:

- The usage of various orders of Taylor terms directly affects deflection and stress results.

- There is no fluctuation on deflection results of 0^{th} and 4^{th} order terms, which gives good accuracy with respect to analytical solution.
- Less fluctuated stress values are obtained with the usage of 0^{th} order Taylor series terms in NI-RPIM when no stabilization method is used.
- Fluctuations on stress results are decreased with the usage of ASD and LSS methods.
- 0^{th} order term results of NI-RPIM with ASD gives the best stress results and less fluctuation values in the solutions.
- High stress fluctuations on boundaries where essential boundary conditions are applied can be decreased with changing local stiffness values of corresponding nodes.
- Support domain size (sd) can affect stress results of NI-RPIM with ASD method.
- Changes of alfc (α_c) with ASD method do not have significant effect on NI-RPIM stress results in the regions where the essential boundary conditions are not included. Different values of q show similar stress distribution characteristics on NI-RPIM with ASD method.

References

Atluri, S. N. and Zhu, T. (1998) A new meshless local Petrov-Galerkin (MLPG) approach in computational mechanics, *Computational Mechanics* **22,** 117-127.

Babuska, I. and Melenk, J. (1996) The partition of the unity finite element method: basic theory and applications, *Comput. Methods Appl. Mech. Engrg.* **139**, 289-314.

Belytschko, T., Lu, Y. Y. and Gu, L. (1994) Element-free Galerkin methods, *Int J Numer Methods Eng* **37**, 229-256.

Beer, F. P., Johnston-Jr, E. R., Dewolf, J. T. and Mazureket, D. (2009). *Mechanics of Materials*. (5^{th} edn.) McGraw-Hill Press, Singapore.

Bhowmick, S. and Shontz, S. M. (2012) Towards high-quality, untangled meshes via a force-directed graph embedding approach. *Procedia Computer Science*, **1**, 357–366.

Biessel, S. and Belytschko, Y. (1996) Nodal integration of the element-free Galerkin method, *Comput. Methods Appl. Mech. Engrg.* **139**, 49-74.

Bonet, J. and Kulasegaram, S. (2000) Finite increment gradient stabilization of point integrated meshless methods for elliptic equations, *Communications in Numerical Methods in Engineering* **16**, 475–483.

Bozkurt, O. Y., Kanber, B. and Asik, M. Z. (2013) Assessment of RPIM shape parameters for solution accuracy of 2D geometrically nonlinear problems, *International Journal of Computational Methods* **10(3)**, 1-26.

Chen, J., Wu, C., Yoon, S. and You, Y. (2001) A stabilized conforming nodal integration for Galerkin mesh-free methods, *International Journal for Numerical Methods in Engineering* **50**, 435-466.

Chen, W. and Tanaka, M. (2002) Meshless, integration-free, and boundary-only rbf technique, *Computers and Mathematics with Applications* **43**, 379-391.

Duan, Q. and Belytschko, T. (2008) On the stabilization of stress-point integration in the Element Free Galerkin method, *Meshfree Methods for Partial Differential Equations IV Lecture Notes in Computational Science and Engineering* **65**, 47-68.

Elmer, W., Chen, J. S., Puso, M. and Taciroglu, E. (2012) A stable meshfree nodal integration method for nearly incompressible solids, *Finite Elements in Analysis and Design* **51**, 81–85.

Fries, T. and Belytschko, T. (2007) Convergence and stabilization of stress-point integration in mesh-free and particle methods, *International Journal for Numerical Methods in Engineering* **74(7)**, 1067-1087.

Gingold, R. A. and Monaghan, J. J. (1977) Smoothed particle hydrodynamics: theory and application to non-spherical stars, *Monthly Notices of the Royal Astronomical Society* **181**, 375-389.

Han, K. (2010) Efficient meshfree analysis Using stabilized conforming nodal integration for metal forming simulation, *Journal of the Korean Society of Marine Engineering* **34(7)**, 943-950.

Kanber, B., Bozkurt, O. Y. and Erklig, A. (2013) Investigation of RPIM shape parameter effects on the solution accuracy of 2D elastoplastic problems, *International Journal for Computational Methods in Engineering Science and Mechanics* **14**, 354–366.

Kovalev, K. (2005) *Unstructured hexahedral non-conformal mesh generation*. PhD thesis, Faculty of Engineering Vrije Universiteit Brussel, Belgium.

Liu, G. R. and Gu, Y. T. (2001) A point interpolation method for two-dimensional solids, *International Journal for Numerical Methods in Engineering* **50**, 937-951.

Liu, G. R. and Zhang, G. Y. (2008) Edge-based smoothed point interpolation methods, *International Journal of Computational Methods* **5(4)**, 621-646.

Liu, G. R. and Zhang, G. Y. (2009) A normed G space and weakened weak (W2) formulation of cell-based smoothed point interpolation method, *International Journal of Computational Methods* **6(1)**, 147-179.

Liu, G. R., Zhang, G. Y., Dai, K. Y., Wang, Y. Y., Zhong, Z. H., Li, G. Y. and Han, X. (2005) A linearly conforming point interpolation method (LC-PIM) for 2D solid mechanics problems, *International Journal of Computational Methods* **2(4)**, 645–665.

Liu, G. R., Zhang, G. Y., Wang, Y. Y., Zhong, Z. H., Li, G. Y. and Han, X. (2007) A nodal integration technique for meshfree radial point interpolation method (NI-RPIM), *International Journal of Solids and Structures* **44**, 3840-3860.

Liu, W. K., Chen, Y., Chang, C. T. and Belytschko, T. (1996) Advances in multiple scale kernel particle methods, *Comput Mech* **18**, 73-111.

Liu, W. K., Ong, J. S. and Uras, R. A. (1985) Finite element stabilization matrices - a unification approach, *Computer Methods in Applied Mechanics and Engineering* **53,** 13–46.

Lucy, L. B. (1977) A numerical approach to the testing of the fission hypothesis, *The Astronomical Journal* **82(12),** 1013-1024.

Nagashima, T. (1999) Node-by-node meshless approach and its applications to structural analysis, *Int. J. Numer. Meth. Engrg.* **46**, 341–385.

Nayroles, B., Touzot, G. and Villon, P. (1992) Generalizing the finite element method: diffuse approximation and diffuse elements, *Comput Mech* **10**, 307-318.

Nguyen-Van, H., Duy, N. M. and Tran-Cong, T. (2007) A simple and accurate four-node quadrilateral element using stabilized nodal integration for laminated plates, *CMC* **6(3)**, 159-175.

Tonon, F. (2004). Explicit exact formulas for the 3-D tetrahedron inertia tensor in terms of its vertex coordinates. *Journal of Mathematics and Statistics*, **1(1)**, 8-11.

Wang, J. G. and Liu, G. R. (2002a) A point interpolation meshless method based on radial basis functions, *International Journal for Numerical Methods in Engineering* **54**, 1623-1648.

Wang, J. G. and Liu, G. R. (2002b) On the optimal shape parameters of radial basis functions used for 2-D meshless methods, *Comput Methods Appl Mech Engrg* **191,** 2611–2630.

Xu, S. (2014) Stable cracking particles method based on stabilized nodal integration and updated Lagrangian kernel, *Mathematical Problems in Engineering* **2014**, 1-10.

Yavuz, M. M. and Kanber, B. (2015) On the usage of tetrahedral background cells in nodal integration of RPIM for 3D elasto-static problems, *International Journal of Computational Methods* (Accepted for publication).

Zhang, G. Y., Liu, G. R., Wang, Y. Y., Huang, H. T., Zhong, Z. H., Li, G. Y. and Han, X. (2007) A linearly conforming point interpolation method (LC-PIM) for three dimensional elasticity problems, *International Journal for Numerical Methods in Engineering* **72**, 1524-1543.

Zhou, J. X., Wen, J. B., Zhang, H. Y. and Zhang, L. (2003) A nodal integration and post-processing technique based on Voronoi diagram for Galerkin meshless methods, *Comput. Methods Appl. Mech. Engrg.* **192**, 3831–3843.